

Structural Properties and Morphology of the Quaternary Semiconductor $\text{AgIn}_4\text{GaTe}_8$

Pérez FV, Gando NJ, Castro JA, Durante Rincón CA, Durán L and Fermin JR*

Departamento de Física, Facultad Experimental de Ciencias, Universidad del Zulia, Venezuela

Abstract

We report on the structural properties and morphology of the quaternary semiconductor $\text{AgIn}_4\text{GaTe}_8$, prepared by direct fusion of stoichiometric mixture of constituent elements. For this, powder X-Ray Diffractometry (XRD) and Scanning Electron Microscopy (SEM) techniques were employed. From the XRD patterns we have identify a tetragonal phase together with a secondary orthorhombic phase. A strain/size analysis of the full-width-half-maximum (FWHM) of the diffraction lines, showed an anisotropic microstructure associated to the presence of microstrains, induced by crystallite size variations combined with crystallite dislocations. The SEM measurements reveal a material with very rough surface and faceted grains. The grain size determined from SEM micrographs was larger than the crystallite size obtained from the XRD data.

Keywords: $\text{AgIn}_4\text{GaTe}_8$; Modified Scherrer equation; Crystallite size; Strain/size analysis; Anisotropic microstructure; Grain size

Introduction

Ternary and quaternary semiconductors provide a natural way of tuning the desired band gap and flexibility to control other material parameters, by changing the relative composition of the pure elements in the alloy. A special group of ternaries includes the families I-III-VI₂ and I-III₅-VI₈ [1,2]. The most studied of the first class of alloys are $\text{Ag}(\text{In,Ga})(\text{Te,Se})_2$ [3-5], which crystallize in the non-centrosymmetric chalcopyrite structure. This is because these compounds appear as promising candidates for infrared nonlinear optical devices, and solar cells applications [6,7]. On the other hand, semiconductors of the family I-III₅-VI₈ with tetragonal or orthorhombic structure depending on the ion of group III, not only have band gaps suitable for optimum energy conversion solar cells, but also thermoelectric properties useful for applications in waste-heat recovery, air conditioning, and refrigeration [8]. Hence, the study of the physical properties of these semiconductor compounds for useful devices, offer the possibility for newer materials developments, especially of many quaternary compounds. More recently, we have paid attention on the crystalline structure and lattice parameters of the quaternary alloys $\text{Ag}(\text{In}_{1-x}\text{Ga}_x)_5\text{Te}_8$ [9]. This is because these quaternary compounds are expected to exhibit intermediary optical, electrical, and thermal response between the ternaries AgIn_5Te_8 and AgGa_5Te_8 . On the other hand, it is known that $\text{Ag}(\text{In,Ga})_5\text{Te}_8$ is easily obtainable because at these concentrations, the constituent elements melt congruently at relatively low temperatures [10]. This information is also of importance, since the electronic and other physical properties for applications may also depend on the growth conditions.

The structure and properties of semiconductor materials are closely related to the morphology and grain size. Understanding this relationship is critically important to many industrial processes. Furthermore, a look inside a grain can give us information on the hierarchy of microstructure in the materials. The main purpose of this work is to study the structural properties and morphology of the semiconductor $\text{AgIn}_4\text{GaTe}_8$. Our samples were prepared by direct fusion of stoichiometric mixture of constituent elements, and then the crystalline structure, lattice parameters, and crystallite size determined by x-ray diffraction (XRD). In addition, the morphology of the sample and grain size were determined using Scanning Electron Microscopy (SEM).

This paper is organized as follows: in Section II we provide a brief description of the sample preparation and characterization methods. In Section III the experimental results and their analysis are presented. A summary of the main results from this study is presented in Section IV.

Experimental

Polycrystalline ingots of $\text{AgIn}_4\text{GaTe}_8$ were prepared by direct fusion of the stoichiometric mixture of the elements of at least 5N purity, following the synthesis program sketched in Figure 1, and according to the phase diagrams reported for the pseudo-binaries $\text{Ag}_2\text{Te-In}_2\text{Te}_3$ [11], and $\text{Ag}_2\text{Te-Ga}_2\text{Te}_3$ [12]. The samples were synthesized inside evacuated quartz ampoules ($\approx 10^{-6}\text{Torr}$). To minimize the risk of explosion due to exothermic reaction between the group III element and Te, the ampoules were heated in a vertical furnace very slowly at 5°C/h up to

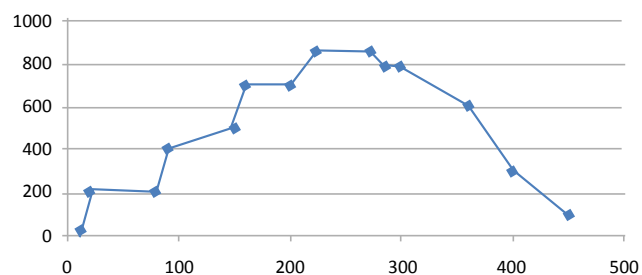


Figure 1: Diagram used for synthesize the quaternary semiconductor $\text{AgIn}_4\text{GaTe}_8$.

*Corresponding author: Fermin JR, Departamento de Física, Facultad Experimental de Ciencias, Universidad del Zulia, Aptdo. Postal 526, Maracaibo 4001, Zulia, Venezuela, Tel: 58 261 7597719; E-mail: jfermin70@gmail.com

Received January 13, 2015; Accepted January 30, 2015; Published February 09, 2015

Citation: Pérez FV, Gando NJ, Castro JA, Durante Rincón CA, Durán L, et al. (2015) Structural Properties and Morphology of the Quaternary Semiconductor $\text{AgIn}_4\text{GaTe}_8$. J Material Sci Eng 4: 154. doi:10.4172/2169-0022.1000154

Copyright: © 2015 Pérez FV, et al. This is an open-access article distributed under the terms of the Creative Commons Attribution License, which permits unrestricted use, distribution, and reproduction in any medium, provided the original author and source are credited.

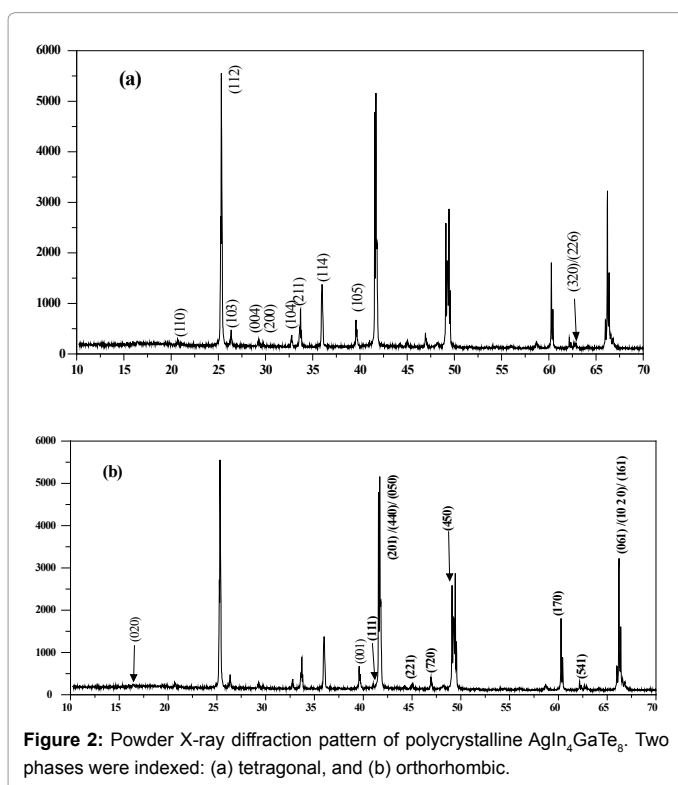
858°C. Kept at this temperature for 48 h, the samples were rocked at regular intervals to achieve a homogeneous mixing of the liquid phase of the reacting mixture, and then cooled to room temperature at a rate of 5°/h.

Powder X-ray diffraction measurements were performed using a diffractometer Bruker D8 Focus with the CuK characteristic line (1.5405 Å) in the Bragg-Brentano geometry. The patterns were collected in the range $10^\circ \leq 2\theta \leq 70^\circ$ with a step size of 0.02 and step time of 40 sec. The diffraction spectrum was then analyzed by using the program WINPLOTR. The microstructure was imaged using a scanning electron microscope (SEM) QUANTA 200FEG microscope, with acceleration potential of 15.0 KeV, and magnifications 16000X and 60000X.

Results and Analysis

Crystalline structure

The X-ray diffraction pattern of $\text{AgIn}_4\text{GaTe}_8$ is shown in Figure 2. Our analysis reveals the presence of at least two different phases. A tetragonal phase (Figure 2a), with unit cell parameters $a=6.070$ Å, $c=12.224$ Å, $c/a=2.0138$, and a secondary phase (Figure 2b) taking place in the orthorhombic structure with unit cell parameters $a=6.274$ Å, $b=10.793$ Å, $c=14.498$ Å. Although in a recent work we have shown that polycrystalline $\text{Ag}(\text{In}_{1-x}\text{Ga}_x)_5\text{Te}_8$ may exhibit a single tetragonal structure for all x values [9], the presence of these two phases in $\text{AgIn}_4\text{GaTe}_8$ is not surprising, since other authors have report that the ternary AgGa_5Te_8 can crystallize in both tetragonal and orthorhombic structure [8,13]. The unit cell parameters obtained for the tetragonal phase in our sample depart from the values $a=6.1503$ Å, $c=12.329$ Å, and $c/a=2.0046$, reported for single-tetragonal $\text{AgIn}_4\text{GaTe}_8$ [9]. This represents a change in the unit cell volume of about 0.034%. It is also noted that there are no restrictions on the order of the allowed

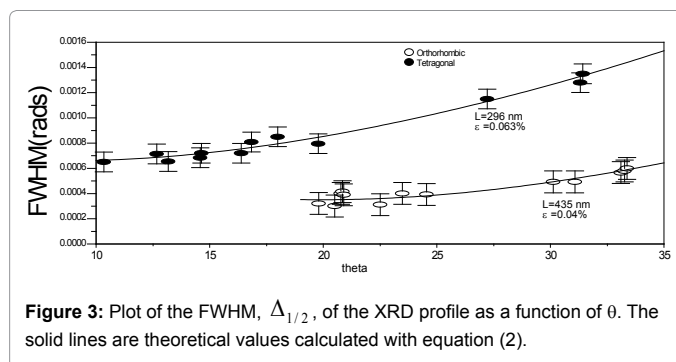


<i>hkl</i>	$2\theta_{\text{obs}}$ (°)	$2\theta_{\text{calc}}$ (°)	<i>d</i> (Å)
110	20.725	20.675	4.2824
112	25.334	25.333	3.5129
103	26.348	26.321	3.3798
004	29.210	29.199	3.0549
200	29.369	29.402	3.0387
104	32.780	32.782	2.7299
211	33.796	33.792	2.6501
114	35.997	36.047	2.4929
105	39.682	39.713	2.2696
108	62.644	62.643	1.4818
226	62.862	62.839	1.4772

Table 1: Powder XRD data of $\text{AgIn}_4\text{GaTe}_8$ obtained for the tetragonal phase in polycrystalline $\text{AgIn}_4\text{GaTe}_8$.

<i>hkl</i>	$2\theta_{\text{obs}}$ (°)	$2\theta_{\text{calc}}$ (°)	<i>d</i> (Å)
0 2 0	16.410	16.412	5.3975
0 0 1	39.582	39.606	2.2750
1 1 1	41.018	41.008	2.1986
2 0 1	41.571	41.595	2.1707
4 4 0	41.693	41.697	2.1646
0 5 0	41.812	41.813	2.1587
2 2 1	45.004	44.999	2.0127
7 2 0	46.940	46.954	1.9341
4 5 0	49.100	49.081	1.8540
1 7 0	60.172	60.317	1.5342
5 4 1	62.172	62.206	1.4919
0 6 1	66.213	66.189	1.4103
1 6 2	66.574	66.542	1.4035
10 2 0	66.769	66.757	1.3999

Table 2: Summary of the data obtained from the Jeffries planimetry.



reflections in both phases (any hkl), so we assume a simple-tetragonal and simple-orthorhombic lattices, respectively. The complete XRD data of $\text{AgIn}_4\text{GaTe}_8$ obtained from our analysis are summarized in Tables 1 and 2.

Crystallite and grain size

The grain size is often related to the full width half maximum (FWHM) of the diffraction pattern, by means of the well-known Scherrer formula [14],

$$\beta = \frac{K\lambda}{L \cos \theta}, \quad (1)$$

where β is the FWHM in rads, $K=2[\ln(2)/\pi]^{1/2}0.93$ is a constant related to the grain shape, λ is the X-ray wavelength in Å, L the average size of the crystallites in Å, and θ the Bragg angle in degrees. Unfortunately,

this method is unreliable estimating grain size, because the assumption that the crystallite size matches the grain size is not always valid at the microscale. A grain may be made up of several different crystallites. In this case, the size effects could be overwhelmed by an anisotropic microstructure.

In Figure 3 we show a plot of the FWHM, β , of the XRD profile as a function of θ , for each phase. The values of β were determined assuming a Gaussian diffraction line, with FWHM given by the equation [15]

$$\beta^2 = \left(\frac{K\lambda}{L \cos \theta} \right)^2 + (4\varepsilon \tan \theta)^2 + \beta_{inst}^2, \quad (2)$$

where β_{inst} is the instrumental contribution to the FWHM, ε an anisotropy constant due to the microstrains, which is dependent on the density of dislocations and crystallite size variations [16]. The instrumental broadening is parametrized from a reference silicon data using the Caglioti's formula [17]

$$\beta_{inst}^2 = U \tan^2 \theta + V \tan \theta + W, \quad (3)$$

where U, V , and W , are scalars. Equation (2) is also referred in the literature as a modified form of the Scherrer formula. With this, we are able to compute the strain/size effects as different sources of broadening for each phase, independently. The solid curves in Figure 3 are least-square fits of the experimental data with equation (2). A reasonable agreement is obtained for crystallite sizes of the order of $L_{tetra} \cong 2960 \text{ \AA} = 296 \text{ nm}$, and $L_{ortho} \cong 4350 \text{ \AA} = 435 \text{ nm}$, and anisotropy constants $\varepsilon_{tetra} \cong 0.063\%$ and $\varepsilon_{ortho} \cong 0.04\%$. This behavior is generally observed in polycrystalline specimens with anisotropic microstructure. For such a material, the crystallite size is an anisotropic quantity: the crystallite size is different along different crystalline directions, and then, an anisotropic size broadening occurs. This size fluctuation is usually

$R(\text{mm})$	$A(\text{mm}^2)$	N_{in}	$N_{intersected}$	$G(\mu\text{m})$
185	107466.5	40	22	6.0
75	17662.5	33	23	6.3
65	13097.5	27	18	6.5
50	7850	19	13	6.7

Table 3: Powder XRD data of $\text{AgIn}_4\text{GaTe}_8$ obtained for the orthorhombic phase in polycrystalline $\text{AgIn}_4\text{GaTe}_8$.

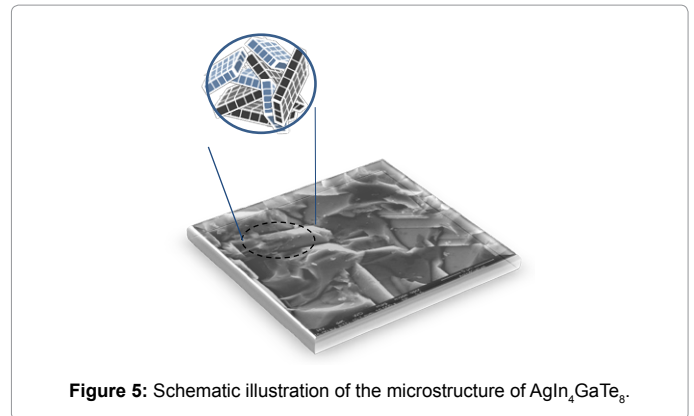


Figure 5: Schematic illustration of the microstructure of $\text{AgIn}_4\text{GaTe}_8$.

accompanied by strain anisotropy induced by crystallite dislocations along the different directions in the specimen.

In Figure 4 we present SEM images of $\text{AgIn}_4\text{GaTe}_8$. These micrographs reveal a very rough surface exhibiting relatively large grains. Furthermore, many of the grains are faceted. The grain size was estimated from these images using the Jeffries planimetric method of ASTM E112 standard [18]. The procedure consists in superimpose test circles of different radii over the microstructure, and then count the grains completely inside, N_{in} , and those grains intersected by the circumference, $N_{intersected}$ (Figure 4c). The grain size is then given by

$$G = \frac{\ln(N_A)}{\ln 2}, \quad (4)$$

where N_A is the number of grains per mm^2 given by

$$N_A = f(N_{in} + 0.5N_{intersected}), \quad (5)$$

$f = M^2/A$ is the Jeffries multiplier, M is the magnification, and A is the area of the circle. Several counts were performed within test circles of radii 50, 65, 75, and 185 mm, over the 16000X image. The results obtained from this planimetric process are resumed in Table 3. From these data we have determined an average grain size, G , of the order of $\sim (6.38 \pm 0.30)\mu\text{m}$. This value is larger than the crystallite sizes obtained from the XRD analysis. Then, according to our results, each of these grains is composed of several tetragonal and orthorhombic crystallites, with different sizes distributed along all directions, and crystallite dislocations within the grain. This picture is illustrated in Figure 5.

Although further work is needed in other to understand the relationship between crystalline structure and the morphology of $\text{Ag}(\text{In}_{1-x}\text{Ga}_x)_5\text{Te}_8$, the results presented here are important for possible applications of these materials in many semiconductor processes.

Summary

Powder XRD and SEM techniques were used to study the structural properties and morphology of polycrystalline $\text{AgIn}_4\text{GaTe}_8$, prepared by

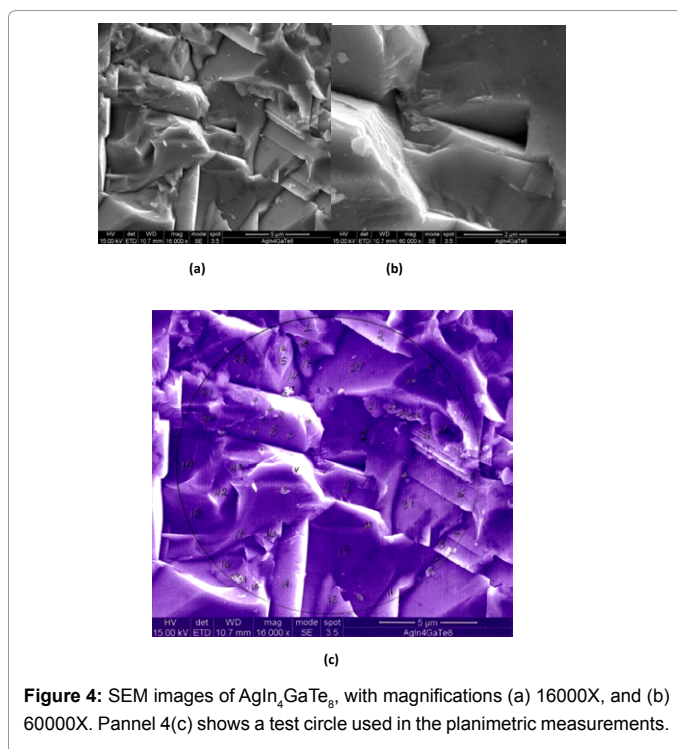


Figure 4: SEM images of $\text{AgIn}_4\text{GaTe}_8$, with magnifications (a) 16000X, and (b) 60000X. Panel 4(c) shows a test circle used in the planimetric measurements.

direct fusion of the stoichiometric mixture of the elements. The XRD patterns showed the coexistence of a tetragonal and an orthorhombic phase. How the coexistence of two coherent crystalline phases affect the physical properties of this system still a matter of further systematic research. The experimental FWHM of the diffraction lines as functions of the diffraction angle, display a behavior consistent with a modified-type Scherrer's equation, involving microstrains due to an anisotropic crystallite size together with crystallite dislocations. This strain/size effect is particularly strong in the tetragonal phase. The average grain size, determined from Jeffries planimetry on the SEM micrographs, was larger than the crystallite size obtained from the XRD patterns. This is an indicative that the grains in this material are made-up of several crystallites. Finally, we emphasize that our discussion is mainly qualitative and in the context of previous results reported in I-III₅-VI₈ semiconductors, and may be taken as a mean of calling attention to the amount of interesting new physics that need further experimental and theoretical investigation in quaternary $\text{Ag}(\text{In}_{1-x}\text{Ga}_x)_5\text{Te}_8$ alloys.

Acknowledgment

The authors gratefully acknowledge the Venezuelan institutions CONDES-LUZ for the financial support (Grant # CC-0595-10) and FONACIT (Contract 201100542).

References

1. Roy UN, Mekonen B, Adetunji OO, Chattopahyay K, Kochari F (2002) Compositional variations and phase stability during horizontal Bridgman growth of AgGaTe_2 crystals. J Crys Growth 241: 135-140.
2. Delgado GE, Mora AJ (2009) Structural Characterization of the Semiconductor Chalcogenide System Ag-In-VI (VI = S, Se, Te) by X-Ray Powder Diffraction. Chalcogenide Lett 6: 635-639.
3. Burger A, Ndap JO, Cui Y, Roy U, Morgan S (2001) Preparation and thermophysical properties of AgGaTe_2 crystals. J Crystal Growth 225: 505-511.
4. Xue D, Betzler K, Hesse H (2000) Dielectric properties of I-III-VI₂-type chalcopyrite semiconductors. Phys Rev B 62: 13546-13551.
5. Bellabarba C (1998) Electrical properties of AgInTe_2 . Matter Lett 36: 299-302.
6. Matsushita H, Takashi M, Katsui A, Takizawa T (2000) Thermal analysis and synthesis from the melts of Cu-based quaternary compounds Cu-III-IV-VI₄ and Cu₂-II-IV-VI₄ (II=Zn, Cd; III=Ga, In; IV=Ge, Sn; VI=Se). J. Crys. Growth 208: 416-422.
7. Krustok J, Jagomägi A, Grossberg M, Raudoja J, Danilson M (2006) Photoluminescence properties of polycrystalline AgGaTe_2 . Solar Energy Materials & Solar Cells 90: 1973-1982.
8. Charoenphakdee A, Kurosaki K, Muta H, Uno M, Yamanaka S (2009) Thermal Conductivity of the ternary compounds: AgMTe_2 and AgM_5Te_8 (M=Ga or In). Materials Transactions 50: 1603-1606.
9. Durante C, Castro J, Durán L, Fermin JR (2013) Structural, thermal and optical properties of $\text{Ag}(\text{In}_{1-x}\text{Ga}_x)_5\text{Te}_8$. Materials Science: An Indian Journal .In press.
10. Sánchez A, Meléndez L, Castro J, Hernández JA, Hernández E (2005) Structural, optical, and electrical properties of AgIn_3Te_8 . J Appl Phys 97: 053505.
11. Chiang PW, O'Kane DF, Mason DR (1967) Phase Diagram of the Pseudo-Binary System $\text{Ag}_2\text{Te} - \text{In}_2\text{Te}_3$, and Semiconducting Properties of $\text{AgIn}_9\text{Te}_{14}$. J Electrochem. Soc 114: 759-760.
12. Guittard M, Rivet J, Mazurier A (1988) Systeme $\text{Ag}_2\text{Te}-\text{Ga}_2\text{Te}_3$. Phases intermediaries. Determinations structurales. Diagramme de Phase Mat Res Bull A 23: 217.
13. Julien C, Ivanov A, Khelifa A, Alapini A, Guittard M (1996) Characterization of the ternary compounds AgGaTe_2 and AgGa_5Te_8 . J of Mat Science 31: 3315-3319.
14. Patterson AL (1939) The Scherrer Formula for X-Ray Particle Size Determination. Phys. Rev 56: 978.
15. Balzar D, Popovic S (1996) Reliability of the Simplified Integral-Breadth Methods in Diffraction Line-Broadening Analysis. J Appl Cryst 29: 16-23.
16. K, Lahiri D (2004) X-ray diffraction line profile analysis for defect study in Zr-2.5% Nb material. Bull Mater Sci 27: 59-67.
17. Caglioti G, Paoletti A, Ricci FP (1960) On resolution and luminosity of a neutron diffraction spectrometer for single crystal analysis. Nucl. Instrum. Methods 9: 195-198.
18. ASTM E (1996) Standard Test Methods for Determining Average Grain Size. Annual Book of ASTM Standards 3: 112.